COMPUTATIONAL FLUID DYNAMICS STUDY OF NASAL CAVITY MODEL

VIZY NAZIRA BINTI RIAZUDDIN

UNIVERSITI SAINS MALAYSIA

2011

COMPUTATIONAL FLUID DYNAMICS STUDY OF NASAL CAVITY MODEL

by

VIZY NAZIRA BINTI RIAZUDDIN

Thesis submitted in fulfillment of the requirements

for the degree of

Master of Science

UNIVERSITI SAINS MALAYSIA

July 2011

ACKNOWLEDGEMENT

Alhamdulillah. Thanks and glory be to Allah (SWT) alone, for giving me this opportunity, strength and patience to complete my dissertation finally, after all the challenges and difficulties.

First and foremost, I would like to express my deepest appreciation to my supervisor; Dr. Kamarul Arifin bin Ahmad, whose encouragement, guidance and support from the very beginning which enabled me to develop the understanding of the subject.

My sincere thanks to Prof. Dr. Zulkifly Abdullah, Prof. Dr. Ibrahim Lutfi Shuaib, Dr. Rushdan Ismail, Assoc. Prof. Dr. Suzina Sheikh Abdul Hamid, and Mr. Mohamad Zihad Mahmud for their continuous thoughtful advice in bringing this research works to fruition. I would like to acknowledge my research colleague, Mr. Mohammed Zubair for his invaluable assistance and support throughout the entire research. I would like to thank all my colleagues for the joyful memories throughout the research.

Special thanks to Mohd Shahadan Mohd Suan, Khairunisa Zulkurnain and my parents, Riazuddin Ahmad Ali and Norizan Osman for their support and encouragement that enabled me to endure the hardship of my academic career.

TABLE OF CONTENTS

ACKNOWLEDGEMENT ii

TABLE OF CONTENTS iii

LIST OF TABLES vii

LIST OF FIGURES viii

LIST OF ABBREVIATIONS xii

LIST OF SYMBOLS xiv

ABSTRAK xvi

ABSTRACT xviii

CHAPTER 1 – INTRODUCTION

1.1 Research Background 1

1.2 Aims and Objectives 3

1.3 Scope of Work 4

1.4 Organization of The Thesis 4

CHAPTER 2 – LITERATURE RIVIEW

2.1 Overview 5

2.2 Anatomy and Physiology of The Human Nasal Cavity 5

2.2.1 Nasal Anatomy 5

2.2.2 Nasal Physiology 8

2.3 Objective measurement methods 9

2.3.1 Rhinomanometry 9

2.3.2 Acoustic Rhinomanometry 10

2.4 Numerical Study of Flow Through The Nasal Cavity 11

2.5 Gender Comparison 19

2.6 Gravity Effect 20

2.7 Plug Flow and Pull Flow Boundary Condition 21

2.8 Summary 22

CHAPTER 3 – MODELLING THE HUMAN NASAL CAVITY

3.1 Overview 23

3.2 3D Computational Model of the Nasal Cavity 24

3.2.1 Procuring CT Scan Data of Human Nasal Cavity 24

3.2.2 Convert 2D CT Scan Images to 3D CAD Data Using Mimics 25

3.2.3 Geometry Creation Using CATIA 28

3.3 Mesh Generation Using GAMBIT 31

3.4 Numerical analysis 33

3.4.1 Governing Equation 33

3.4.2 Turbulence Models 34

3.4.3 Numerical Solver Procedure 35

3.4.4 Boundary Condition Definition 37

CHAPTER 4 – RESULTS AND DISCUSSION

4.1 Overview 39

4.2 Grid Dependency Analysis 39

4.3 Geometry Comparison 41

4.4 Model Comparison 44

4.5 Basic Flow Studies 46

4.5.1 Reynolds Number Calculation 46

4.5.2 Velocity 47

4.5.3 Pressure 50

4.5.4 Wall Shear Stress 51

4.5.5 Inspiration Vs Expiration 54

4.5.5.1 Velocity and Pressure Comparison 54

4.5.5.2 Resistance 56

4.5.5.3 Wall Shear Stress 57

4.6 Various Breathing Rates for Inspiration and Expiration 59

4.6.1 Average Velocity 59

4.6.2 Wall Shear Stress 62

4.7 Preliminary Work On Gender Comparison 65

4.7.1 Geometry Comparison 65

4.8 Gravity Effect On Nasal Airflow Due to the Change Of Posture 72

4.9 Effect of Different Boundary Condition On Flow Parameters 76

4.9.1 Nasal Resistance Comparison for Plug-Flow and Pull-Flow 77

4.9.2 Velocity 79

4.9.3 Pressure 81

4.9.4 Wall Shear Stress 82

CHAPTER 5 – CONCLUSION

5.1 Introduction 84

5.2 Major Conclusions Drawn From This Study 84

5.2.1 Basic Airflow Studies 85

5.2.2 Various Breathing Rates for Inspiration and Expiration 86

5.2.3 Gravity Effect On Nasal Airflow Due to the Change Of Posture 86

5.2.4 Effect of Different Boundary Condition On Flow Parameters 87

5.3 Future Works 88

REFERENCES 90

LIST OF PUBLICATIONS 95

LIST OF TABLES

		Page
Table 3.1	Boundary condition for pull flow and plug flow	37
Table 4.1	The total length of the nasal cavity based on the gender comparison	66
Table 4.2	Characteristic description of nasal cavity for male and female nasal cavity models	69

LIST OF FIGURES

		Page
Figure 2.1	Diagram of the Nasal Cavity- reproduced from the Gray's anatomy of the human body, reproduced from Henry Gray, (1918)	6
Figure 2.2	Coronal section of the main nose airway- reproduced from Zamankhan *et al*.,(2006)	7
Figure 2.3	Simplified structure of the nasal cavity- reproduced from Tsui Wing Shum, (2009)	7
Figure 2.4	Nose-like model- reproduced from Elad *et al*., (1993)	12
Figure 2.5	Medial slide of the tree-dimensional finite element mesh of the right nasal cavity- reproduced from Keyhani *et al*., (1995)	13
Figure 2.6	Computational meshes for subjects A, 12, 14 and 18. Nostrils are shown in blue on the right side of the models and the nasopharynx is on the left- reproduced from Segal *et al*., (2008)	14
Figure 2.7	Nasal cavity model constructed by Wen *et al*., (2008)	15
Figure 3.1	Coronal CT scan images along the axial distance of the human nasal cavity	25
Figure 3.2	CT scan images from A: axial, B: coronal and C: sagittal plane and 3D model of the female human nasal cavity	26
Figure 3.3	Polyline data of the 3D human nasal cavity	28
Figure 3.4	Steps involved in developing 3D model of the nasal cavity using CATIA	30
Figure 3.5	3D computational model of the nasal cavity with surface geometry	31
Figure 3.6	Volume mesh of the 3D computational model of human nasal cavity	32
Figure 3.7	Pressure-based solution method (Fluent User manual)	36

Figure 4.1	Grid independence plot	40
Figure 4.2	Ten cross section area along the axial distance of the nasal cavity	41
Figure 4.3	Ten cross section area through the nasal cavity	42
Figure 4.4	The comparison of cross-sectional area vs. axial distance from anterior to the posterior of the nasal cavity	43
Figure 4.5	Pressure drop vs. inspiratory flow rates compared with previous data	45
Figure 4.6	Average velocity contour along the nasal cavity	48
Figure 4.7	Variation of average velocity along the length of the nasal cavity	49
Figure 4.8	Flow recirculation at the olfactory region	49
Figure 4.9	Comparison between left and right nasal cavity	50
Figure 4.10	Average static pressure along the nasal cavity during inspiration	51
Figure 4.11	Maximum wall shear stress along the axial distance of the nasal cavity (full model)	52
Figure 4.12	Average wall shear stress contour	53
Figure 4.13	Maximum wall shear stress across left and right nasal cavity	54
Figure 4.14	Velocity profile comparison during inspiration and expiration	55
Figure 4.15	Average static pressure along the axial length of the nasal cavity	56
Figure 4.16	Pressure drop value during inspiration and expiration for various flow rates	57
Figure 4.17	Maximum wall shear stress along the axial distance of the nasal cavity	58
Figure 4.18	Average velocity at different flow rates from 7.5 to 40	60

	L/min during inspiration	
Figure 4.19	Model of the nasal cavity showing the olfactory plane	61
Figure 4.20	Average velocity at different flow rates from 7.5 to 40 L/min during expiration	62
Figure 4.21	Maximum wall shear stress values through the axial distance of the nasal cavity during inspiration	63
Figure 4.22	Maximum wall shear stress values through the axial distance of the nasal cavity during expiration	64
Figure 4.23	The comparison of cross section area through the nasal cavity of the human male and female subjects	66
Figure 4.24	The pressure drop value across the nasal cavity	68
Figure 4.25	Variation of Average static pressure with posture	73
Figure 4.26	Effect of change of posture on velocity at 15L/min	73
Figure 4.27	Variation in Max. Wall shear stresses with change of posture	74
Figure 4.28	A: Sitting B: Supine, shows flow variations along a horizontal plane at middle meatus region	75
Figure 4.29	Plug flow boundary condition for inspiration A and expiration B	76
Figure 4.30	Pull flow boundary condition for inspiration A and expiration B	76
Figure 4.31	Nasal Resistance for different airflow rate	77
Figure 4.32	Inspiratory nasal resistance for 15L/min at vestibule, nasal valve, middle section and nasopharynx	78
Figure 4.33	Velocity plot along the axial distance (at 15 L/min)	79
Figure 4.34	Velocity profile for pull flow boundary condition A and plug flow boundary condition B	80
Figure 4.35	Pressure plot for plug and pull flow boundary condition during inspiration A and expiration B	82

Figure 4.36 Maximum wall shear stress values during inspiration 83

LIST OF ABBREVIATIONS

3D	Three Dimensional
AMDI	Advanced Medical and Dental Institute
AR	Atrophic Rhinitis
AAR	Active Anterior Rhinometry
CAD	Computational Aid Design
CAT	Computerized Axial Tomography
CFD	Computational Fluid Dynamics
CPU	Central Processing Unit
CT	Computed Tomography
DSE	Digitized Shape Editor
EIM	Eddy Interaction Model
ENT	Ear, Nose and Throat
HU	Hounsfield Units
IBM	International Business Machines
IGES	Initial Graphics Exchange Specification
LES	Large Eddy Simulation

MRI	Magnetic Resonance Imaging
NAR	Nasal Airway Resistance
OSA	Obstructive Sleep Apnea
RAM	Random-Access Memory
RANS	Reynolds Average Navier Stoke
SST	Shear Stress Transport Model
STP	STEP File/Standard for the Exchange of Product File

LIST OF SYMBOLS

ROMAN SYMBOLS

d	Diameter of the nasal inlet
k	Turbulent kinetic energy
Re	Reynolds number
R	Resistance
S_Φ	The source term of Φ
t	Time
u	Velocity vector
V	Velocity of the flow
y	The distance to the wall
u_τ	Friction velocity
v	Kinematic viscosity of the fluid flow

GREEK SYMBOLS

Γ	Diffusion coefficient
∂	Partial differential equation
Φ	General scalar
ε	Dissipated rate of k
ω	Specific rate of dissipation of k
ρ	Fluid density
μ	Dynamic viscosity of the air

ΔP Pressure drop

SUBSCRIPTS

vel Velocity

SUPERSCRIPT

+ Variable expressed in wall units

KAJIAN PENGKOMPUTERAN DINAMIK BENDALIR TERHADAP MODEL RONGGA HIDUNG

ABSTRAK

Pemahaman terhadap sifat-sifat aliran udara di dalam rongga hidung adalah sangat penting dalam menentukan fisiologi hidung dan dalam membantu diagnosis penyakit yang berkaitan dengan hidung. Setiap manusia mempunyai anatomi rongga hidung yang berbeza. Perubahan dari segi morfologi fisiologi hidung manusia juga telah ditentukan berdasarkan jantina. Terdahulu, tiada sebarang kajian pemodelan numerik yang khusus telah dilakukan bagi membanding serta memastikan pengaruh jantina terhadap pembolehubah aliran dalam rongga hidung. Tambahan pula, pelbagai langkah pemudahan yang berkaitan dengan perubahan postur badan dan penetapan keadaan persempadanan telah diambil bagi melaksanakan pemodelan numerik sehingga mempengaruhi hasil kajian pengaliran udara. Oleh itu, dalam kajian ini, permodelan rongga hidung dalam bentuk tiga dimensi telah dibangunkan dengan menggunakan imej tomografi milik individu perempuan Malaysia yang sihat. Sebuah kesinambungan keadaan mantap dan persamaan *Navier Stoke* telah diselesaikan dalam kedua-dua mekanisme inspirasi dan ekspirasi dengan tingkat aliran di antara 7.5-15 L/min sebagai laminar manakala nilai tingkat aliran di antara 20-40 L/min telah disimulasikan dalam keadaan aliran turbulen. Analisis menggunakan pengkomputeran dinamik bendalir (CFD) menghasilkan visualisasi yang sangat efektif terhadap ciri-ciri aliran di dalam rongga hidung. Nilai tegasan ricih maksimum pada bahagian dinding vestibule

meningkat melebihi 2000 % dengan penigkatan kadar aliran udara daripada 7.5 kepada 40 L/min. Perbandingan di antara mekanisme inspirasi dan ekspirasi serta pengaruh tahap pernafasan yang berbeza terhadap fungsi hidung telah dibentangkan. Anatomi rongga hidung yang kompleks ini telah dicipta bagi memenuhi keperluan fungsi fisiologi dalam membantu proses pernafasan secara normal. Hasil kajian ini telah mengenalpasti beberapa perbezaan anatomi dan fisiologi berdasarkan jantina. Penggunaan pengkomputeran dinamik bendalir telah membantu dalam memahami perbezaan yang wujud berdasarkan jantina yang tidak dapat diukur berdasarkan alat perubatan dan pemerhatian semata-mata. Pengaruh perubahan postur badan terhadap rongga hidung juga telah dikaji. Semasa perubahan posisi duduk kepada posisi baring, purata tekanan statik diperhatikan berubah pada nilai sekitar 0.3%. Perubahan arah graviti akibat daripada perubahan postur badan juga mempunyai pengaruh yang penting terhadap parameter aliran. Kebanyakan penyelidik menggunakan keadaan sempadan *plug flow* dalam menganalisis masalah yang berkaitan dengan aliran di dalam rongga hidung. Kajian ini telah mendedahkan kesilapan dalam menentukan keadaan sempadan dan mendapati wujudnya perbezaan yang jelas di antara hasil kajian yang telah diperolehi daripada kedua-dua kes. Pada bahagian injap rongga, rintangan pada *plug flow* adalah 0.311 Pa-min/L dan 0.147 Pa-min/L pada *pull flow*. Perubahan maksimum nilai rintangan yang berlaku pada bahagian vestibule adalah sebanyak 0.3578 Pa-min/L. Nilai purata halaju pada bahagian vestibule hidung adalah 1.4 m/s ketika *plug flow* dan 0.96 m/s ketika *pull flow*. Nilai purata halaju pada injap rongga pula adalah 1.6 m/s untuk *plug flow* dan 1.41 m/s untuk *pull flow*. Pendekatan yang lebih tepat bagi memodelkan mekanisme fisiologi inspirasi adalah dengan menggunakan model aliran *pull flow*.

COMPUTATIONAL FLUID DYNAMICS STUDY OF NASAL CAVITY MODEL

ABSTRACT

Understanding the properties of airflow in the nasal cavity is very important in determining the nasal physiology and in diagnosis of various anomalies associated with the nose. Inter-human anatomical variation for the nasal cavity exists and also differences on physiological morphology are observed based on gender. No specific numerical modeling studies have been carried out to compare and ascertain the effect of gender on flow variable inside the nasal cavity. Also numerical modeling involves various simplifications, for example the postural effect and appropriate boundary conditions which affect the outcome of the airflow studies. The present work involves development of three-dimensional nasal cavity models using computed tomographic images of healthy Malaysian females. A steady state continuity and Navier stoke equations were solved for both inspiratory and expiratory mechanism with flow rates ranging from 7.5 to 15 L/min as laminar and 20 to 40 L/min studies were simulated depicting turbulent flow conditions. Computational fluid dynamics (CFD) analysis provided effective visualization of the flow features inside the nasal cavity. The comparison between inspiratory and expiratory mechanism and the effect of different breathing rates on nasal function have been presented. The value of maximum wall shear stress at the vestibule region increased by more than 2000 % as the flow rate increased from 7.5 to 40 L/min. The complicated anatomy of the nasal cavity has been naturally designed to attain the physiological function desired to facilitate normal breathing. The

current study has identified certain gender based anatomical and physiological differences. The use of computational fluid dynamic has assisted in the understanding of these differences which could not be earlier quantified based on mere medical observation and measurement devices. The influence of postural changes in nasal cavity has also been investigated. Around 0.3% change in the average static pressure is observed while changing from sitting to supine position. The change in the direction of gravity due to change of posture significantly influences the flow parameters and hence should be considered in all future studies involving nasal flow. Most of the researchers employ plug flow boundary definitions to address the flow problems associated with nasal flow. This study has revealed the fallacy of such a definition and found significant differences in values obtained in either case. Comparative study of the pull flow model and the plug flow model has found significant variations highlighting the need for using the right boundary conditions. At the nasal valve, the resistance for plug flow was 0.311 Pa-min/L and for pull flow the value was 0.147 Pa-min/L. Maximum variation was noticed at the vestibule region with 0.3578 Pa-min/L. The average velocity for nasal vestibule and nasal valve is 1.4m/s and 1.6m/s for plug flow. Whereas, for pull flow case, the average velocity value in nasal vestibule and nasal valve region was observed to be around 0.96m/s and 1.41m/s respectively. A correct approach therefore to the numerical model is the pull flow model, which more directly represents the physiological inspiratory mechanism.

CHAPTER 1

INTRODUCTION

1.1 Research background

Nasal cavity is one of the most important components of human respiratory system. It provides the first line protection for lung by warming, humidifying and filtering the inspired air. The success of nasal function is highly dependent on the fluid dynamics characteristic of airflow through the nasal cavity. Better understanding of airflow characteristic in nasal cavity is essential to understand the physiology of nasal breathing.

Airflow through human nasal passages has been studied numerically and experimentally by a number of researchers (Wen *et al*., 2008; Mylavarapu *et al*., 2009; Segal *et al*., 2008; Weinhold *et al*., 2004). Also, several researchers have undertaken studies pertaining to airflow through nasal cavity using measuring devices such rhinomanometer and acoustic rhinomanometry (Hilberg *et al*., 1989, Sipilia *et al*., 1997, Jones *et al*., 1987, Shelton *et al*., 1992, Suzina *et al*., 2003). Rhinomanometry is used to measure the pressure required to produce airflow through the nasal airway and acoustic rhinomanometry is used to measure the cross sectional area of the airway at various nasal planes. However, measuring the precise velocity of airflow and evaluating the local nasal resistance in every portion of the nasal cavity have proven to be difficult (Ishikawa *et al*., 2006). The anatomical complexity of the nasal cavity makes it difficult for the measurement of nasal resistance. The small sizes of the nasal cavity and its narrow flow passage can cause perturbations in the airflow with any inserted probe.

Moreover, the reliability of the result obtained using this device depends on optimal cooperation from the subject, correct instructions from the investigator, and standardized techniques (Kjærgaard *et al*., 2009). There are reports of failure rates of between 25% and 50% in the subjects examined by rhinomanometry (Austin *et al*., 1994).

Due to the inherent limitations of these measuring devices, Computational Fluid Dynamics (CFD) has been proposed as a viable alternative. CFD which refers to use of numerical methods to solve the partial differential equation governing the flow of a fluid, is becoming an increasingly popular research tool in fluid dynamics. The non-invasive CFD modelling allows investigation of a wide variety of flow situations through human nasal cavities.

In order to investigate the physiology of human nasal function, many researchers have conducted numerical analysis to study the airflow profile in nasal respiration (Wen *et al*., 2008, Mylavarapu *et al*., 2009, Segal *et al*., 2008, Weinhold *et al*., 2004, Xiong *et al*., 2008, Croce *et al*., 2006, Garcia *et al*., 2007). However, most of the researchers employed male human subject in the determination of the nasal patency. Individual variation in nasal cavity anatomy existed and also differences on physiological morphology are observed based on gender. No specific numerical modelling studies have been carried out to compare and ascertain the effect of gender on flow variable inside the nasal cavity. Also CFD modelling involves various simplifications, for example the postural effect which affect the outcome of the airflow studies. Despite of the popularity of CFD in the study of nasal airflow, uncertainty still surrounds the appropriateness of the various assumptions made in CFD modelling, particularly with regards to the definition of boundary condition.

In the present study, inspiratory and expiratory steady airflow numerical simulations were performed using 3D nasal cavity model derived from computed tomography scan images. A comparative study is made of the female nasal cavity flow dynamics with that of the male nasal cavity as determined by other researchers. The effect of gravity on modelling nasal airflow and its effect on wall shear stress are also examined. Also plug and pull flow boundary conditions were compared to evaluate the effect of different boundary conditions on the flow parameters. Studies are carried out for various flow rates of 7.5 L/min, 10 L/min, 15 L/min, 20 L/min, 30 L/min and 40L/min suggesting various breathing rates.

1.2 Aims and Objectives

The overall objective of the present study is focused on the investigation of the airflow characteristic along the nasal airway during inspiration and expiration. The aims include the following objectives:

- To develop a three dimensional nasal cavity using the CT scans data.
- To carry out inspiratory steady state numerical simulation.
- To study the effect of different breathing conditions on the nasal physiology.
- To analyze the effect of different boundary conditions on the flow behavior.
- To investigate the effect of gravity and posture on flow properties inside the nasal cavity.

1.3 Scope of work

This research work was preliminarily performed by procuring CT scan images of human nasal cavity. The CT scan data was provided by Prof Ibrahim Lutfi Shuaib, a radiologist from Advanced Medical and Dental Institute (AMDI), Universiti Sains Malaysia. A normal nasal cavity of 39 year old Malaysian female was selected for the study case. The selected CT scan data was imported into MIMICs in order to process the scan images and to generate an accurate three-dimensional computational-aided design (CAD) model of the nasal airway. This was then followed by 3D surface geometry creation by using CATIA. The 3D nasal cavity model was imported into GAMBIT for mesh generation. Numerical simulation was further carried out by using FLUENT^{TM} and the result obtained was validated with previous published work.

1.4 Organization of the thesis

This thesis contains 5 chapters. The first chapter provides an introduction that reviews relevant research objectives, and related outlines of the purposes of this study. Chapter 2 presents an in-depth review of the background for this research. The chapter begins with an introduction to the anatomy and physiological function of the human nasal cavity and is followed by a review of previous studies related to the research. Chapter 3 presents the method used to construct a three dimensional human nasal cavity from CT scan and approach to CFD simulation. Chapter 4 presents the results obtained from the study cases. Finally, a summary of the results of the various studies and general conclusions reached, as well as suggestions for future work, are presented in Chapter 5.

CHAPTER 2

LITERATURE REVIEW

2.1 Overview

This chapter discusses nasal anatomy and physiology function of the human nasal cavity. The conventional method used in the measurement of the nasal cavity has been highlighted. A brief summary of the numerical modelling studies carried out by other researchers has been presented. The importance of gender comparison, effect of posture and the necessity for adopting the appropriate boundary condition in the numerical analysis of the nasal airflow has been literally evaluated.

2.2 Anatomy and physiology of the human nasal cavity

The anatomy and physiology of the human nasal cavity are presented in this section.

2.2.1 Nasal anatomy

The nose is the only external part of the respiratory system. It is made of bone and cartilage and fibro fatty tissues. As illustrated in Figure 2.11, the nasal cavity is divided into right and left cavities by a thin plate of bone and cartilage called the nasal septum. The nasal cavity lies above the hard plate. The hard portion of the palate forms the floor of the nasal cavity, separating it from the oral cavity below. The two openings in the nose called nostrils, allow air to enter or leave the body during breathing. Just beyond the external naris is a funnel shaped dilated region called the vestibule. The

narrow end of the funnel leads to a region referred to as the nasal valve. The nasal valve is the narrowest region of the nasal passage and has a special significance to the nasal function and nasal airflow pattern (Probst et al., 2006). At the end of the nasal valve the cross-sectional area of the airway increases, which mark the beginning of the main nasal passage (see Figure 2.1).

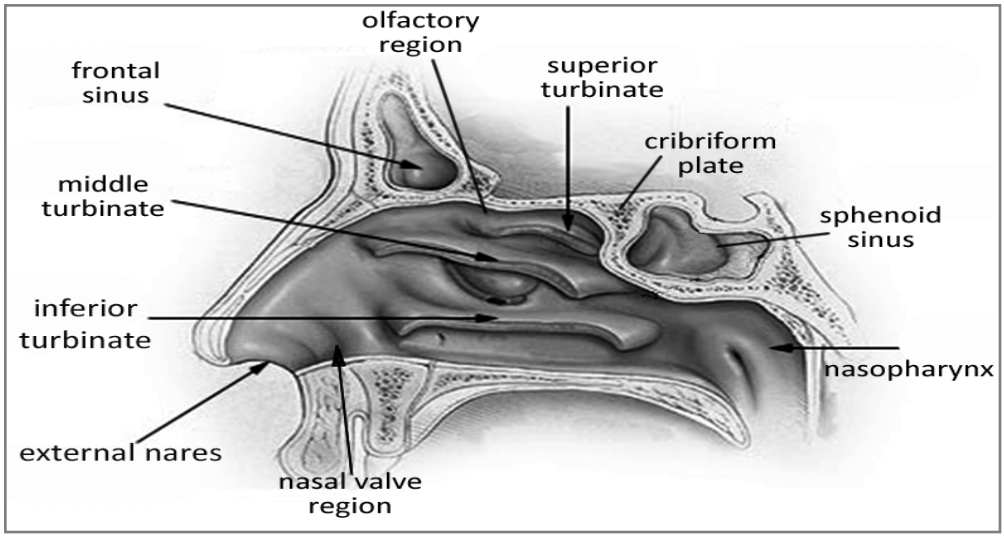

Figure 2.1: Diagram of the Nasal Cavity-reproduced from the Gray's anatomy of the human body, reproduced from Henry Gray, (1918)

On the lateral wall, there are three horizontal projections called turbinate or conchae, which divide the nasal cavity into three air passage. The three turbinates are named as inferior, middle and superior turbinates, according to their position and function (see Figure 2.2). The airway gap in between the turbinates and the central nasal septum walls is the meatus. The meatus are very narrow, normally being about 0.5-1mm. (Proctor and Andersen, 1982). At the posterior end of the main nasal passage, the turbinates and the septum end at the same point. The point at which the two nasal cavities merge into one and marks the beginning of the nasopharynx. At this point, the

cross section area of the airway is reduced and the path of the air-stream bends about 90º downwards towards the trachea (see Figure 2.3).

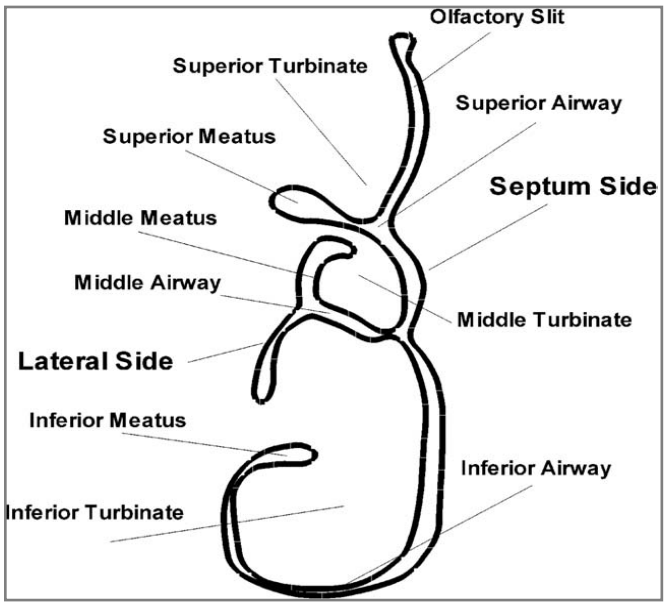

Figure 2.2: Coronal section of the main nose airway- reproduced from Zamankhan et al., (2006)

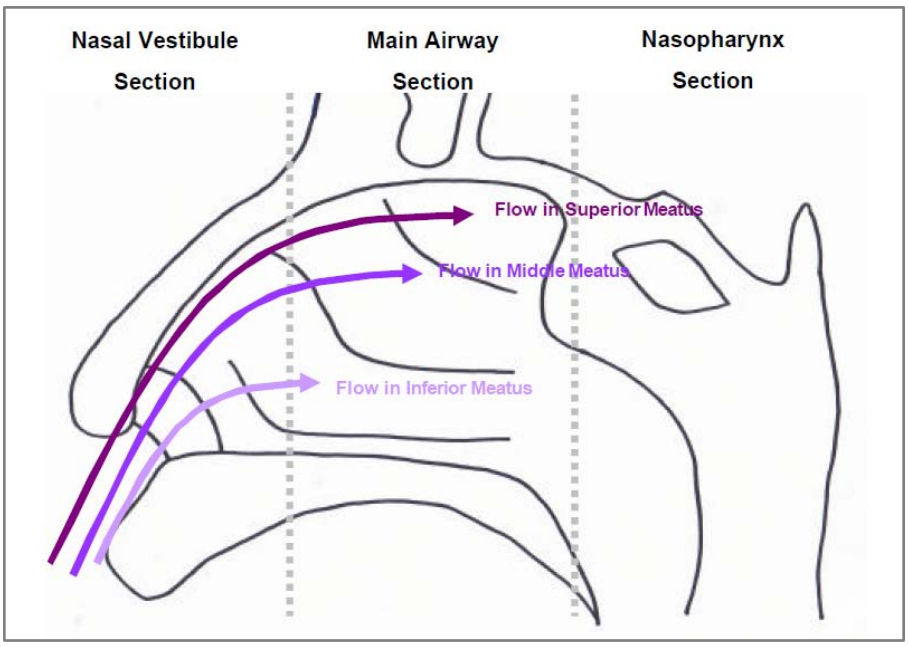

Figure 2.3: Simplified structure of the nasal cavity- reproduced from Tsui Wing Shum, (2009)

2.2.2 Nasal physiology

The human nose has two primary functions. The first is olfaction, the sense of smell. The second function is air-conditioning. Inspired air is conditioned by a combination of heating, humidification and filtering to provide the first line protection for the lung (Elad *et al*., 2008).

The nasal conchae help to slow down the passage air, causing it to swirl in the nasal cavity. The nasal cavity is lined by mucous membrane containing microscopic hairlike structures called cilia. The cells of the membrane produce mucus, a thick gooey liquid. The mucus moistens the air and traps any bacteria or particles of air pollution. Microscopic finger-like projections on the surface of the mucosal cells lining the nasal cavity called cilia. The cilia wave back and forth in rhythmic movement. Cilia will slowly propel the mucus backwards into the pharynx where it is swallowed. The nose is so effective that inspired air is cleared of all particulate matter larger than 6 microns-smaller than the size of a red blood cell.

The nose also acts as the organ of olfaction and has a specially adapted mucosal lining along its roof for this purpose. In order to stimulate the olfactory system (sense of smell), the odorant particles must interact with olfactory receptors located in the olfactory mucosa. Odorants must therefore be capable of being delivered to the olfactory region by inspired air and be able to dissolve sufficiently in the mucus covering the olfactory mucosa (Ishikawa *et al*., 2009).

2.3 Objective measurement methods

Objective measurement methods are the conventional tools utilized by medical practitioners to measure the physiology and anatomy of the nasal cavity. In this section, the main objective measurement methods are discussed namely rhinomanometry and acoustic rhinometry.

2.3.1 Rhinomanometry

Rhinomanometry is a tool which is used to measure nasal airway resistance by making a quantitative measurement of nasal flow and pressure. The European committee of standardization of Rhinomanometry has selected the formula $R = \Delta P/V$ at a fixed pressure of 150Pa; to facilitate comparison of results. (where R=resistance, ΔP=pressure drop, V is the velocity of flow). Rhinomanometry can be performed by anterior or posterior approaches. However this technique is time consuming and requires a great deal of patient cooperation, particularly difficult with children. It cannot be used in the presence of septal perforations and when one or both cavities are totally obstructed. It is affected by nasal cycle and errors as high as 25% are reported for repetitions within 15 minute (Hilberg *et al*., 1989). It cannot accurately assess a specific area of the nasal cavity. Rhinomanometry is time consuming, requires technical expertise, a high degree of subject cooperation and is impossible in subjects with severely congested nasal airways. There are reports of failure rates of between 25% and 50% in the subjects examined by rhinomanometry (Austin *et al*., 1994).

2.3.2 Acoustic Rhinometry (AR)

Acoustic Rhinometry analyses ultrasound waves reflected from the nasal cavity to calculate the cross sectional area at any point in the nasal cavity as well as the nasal volume. Acoustic rhinometry was first described for clinical use in 1989. The list of clinical problems that can be analyzed objectively with acoustic rhinometry has expanded to include turbinoplasty, sleep disorders, more types of cosmetic/reconstructive procedures, sinus surgery, vasomotor rhinitis, maxillofacial expansion procedures, and aspirin and methacholine challenge (Corey, 2006). Acoustic rhinometry is a tool that can aid in the assessment of nasal obstruction. The test is noninvasive, reliable, convenient, and easy to perform. Common clinical and practical uses of acoustic rhinometry for the rhinologic surgeon include assessment of “mixed" nasal blockage, documentation of nasal alar collapse, and preoperative planning for reduction rhinoplasty.

Acoustic rhinometry can also be used to document the positive effect of surgery on nasal airway obstruction (Devyani *et al*., 2004). However, AR may be unreliable due to artifacts (Tomkinson *et al*., 1998) & errors can occur in cross sectional area estimation (Tomkinson *et al*., 1995). Suzina *et al*., (2003) concluded that AAR is a sensitive but not a specific tool for the detection of abnormalities in NAR and it failed to relate to the symptom of nasal obstruction. There is a poor correlation between subjective sensation of nasal airflow and objective measurements (Ecckes, 1998). Reichelmann *et al*., (1999) found unreliability of acoustic rhinometry in pediatric rhinology. Mean cross-sectional areas measured by AR were constantly less than those measured by CT of the nasal cavity up to 33 mm from the nostril, whereas areas measured by AR were greater than

those measured by CT scans beyond that point (Min *et al*., 1995, Mamikoglu *et al*, 2000). AR is not a reliable method for the indication or evaluation of surgery for nasal obstruction (Reber *et al*., 1998).

2.4 Numerical study of flow through the nasal cavity

Better understanding of airflow characteristic in nasal cavity is essential to study the physiological and pathological aspect of nasal breathing. The success of nasal function is highly dependent on the fluid dynamics characteristic of airflow. The anatomical complexity of the nasal cavity makes direct measurements within the nasal cavity highly impossible. CFD has the ability to provide quantitative airflow information at any location within the nasal airway model. These airway models were reconstructed from magnetic resonance (MRI) or computed tomography (CT) imaging data of patients. Recent developments in medical imaging coupled with computational science have opened new possibilities for physically realistic numerical simulations of nasal airflow.

A number of researchers have shown the validity and potential use of CFD in evaluating the flow conditions inside the nasal cavity. Early work regarding this topic was performed by Elad *et al*., (1993) who conducted numerical simulations of steady laminar flow through a simplified nose-like model which resemble the complex anatomy of human nasal cavity using the finite element software package FIDAP (Fluid Dynamics International) (see Figure 2.4). The number of mesh created for this nasal model is approximately <3000 elements. They found that during expiration, flow pattern spread uniformly into nasal cavity until it reached turbinate. The turbinate is an obstacle in the airway that increases the resistance to airflow. The lowest resistance in the model

was located along the floor of the nasal cavity. The flow pattern was also found to be similar during inspiration and expiration but in opposite direction.

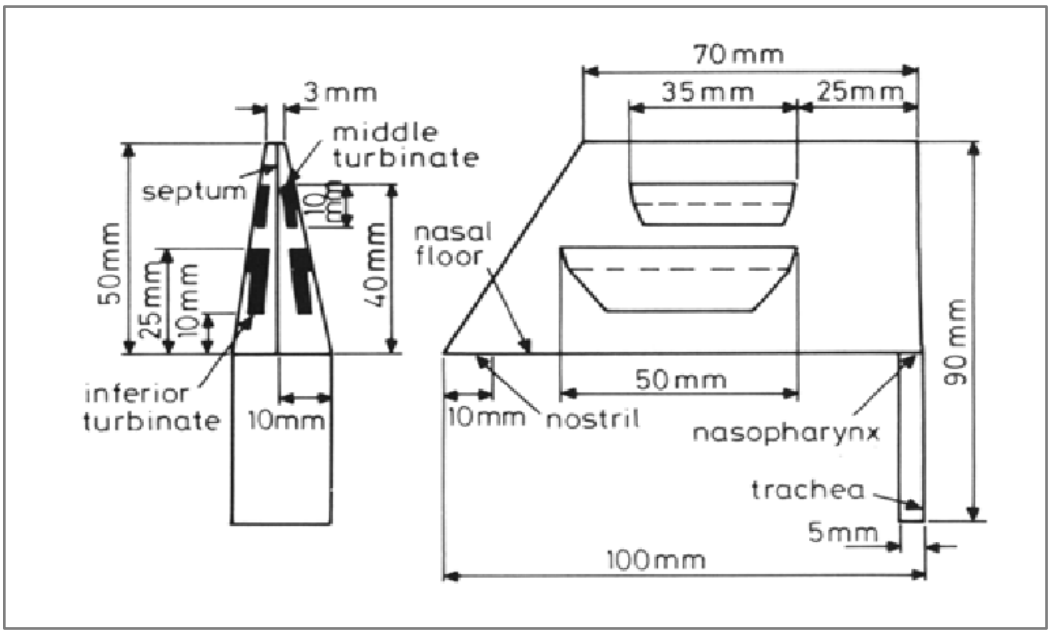

Figure 2.4: Nose-like model- reproduced from Elad et al., (1993)

Due to computational limitation, Naftali *et al*., (1998) in their early work constructed a 2D nose-like model based on averaged data of human nasal cavities to study the transport phenomena of normal and diseased human noses for inspiration under various ambient conditions. They treated the nasal airflow as laminar and simulated the nasal airflow for average breathing rates about 15 m/s with Reynolds number approximately 500. The results demonstrated that the turbinates increase the rate of local heat and moisture transport by narrowing the passageways for air and by induction of laminar swirls downstream of the turbinate wall.

Another early study was that of Keyhani *et al*., (1995) who performed a finite element analysis of steady laminar flow through one side of the human nasal cavity. The

3D nasal model was reconstructed from 42 coronal CAT scans using an imaging software called VIDA (Cardiothoratic Imagaing Research Section, University of Pennsylvania). A computer program was developed in order to convert the coordinate data into a format that could be processed by the mesh generator module of FIDAP. As seen in Figure 2.5, the final domain contained 76,950 brick shape mesh elements.

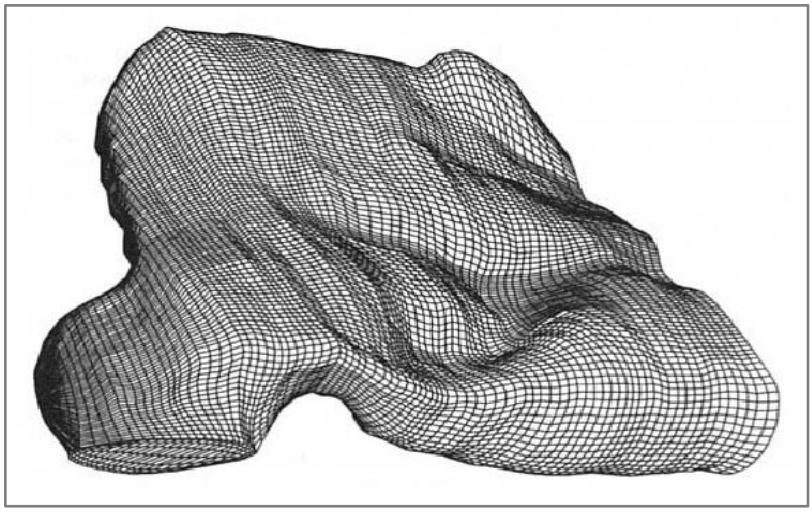

Figure 2.5: Medial slide of the three-dimensional finite element mesh of the right nasal cavity- reproduced from Keyhani et al., (1995)

The laminar flow was simulated for breathing rates of 125 ml/s and 200 ml/s using computational fluid dynamics (CFD) software, FIDAP. Their numerical results were validated with the experimental measurements obtained by Hahn *et al.*, (1993). According to this study, the majority of the airflow passes through the inferior turbinate. Results obtained also confirmed that airflow through the nasal cavity is laminar during quiet breathing.

Airflow in the main nasal cavity is generally described as laminar by several researchers for flow rates of 7.5 L/min to 15 L/min. Segal *et al*., (2008) performed numerical simulation of steady state inspiratory laminar airflow for flow rate of 15 L/min. In their study, three dimensional computational models of four different human nasal cavities which constructed from coronal MRI scans were used (see Figure 2.6). The nasal model then was meshed with hexahedral elements using a semi-automated process MAesh which was developed in-house using Matlab (The MathWorks, Inc., Natick, MA, USA). In their study, they found that in all four nasal models, the majority of flow passed through the middle and ventral regions of the nasal passages. The amount and the location of swirling flow differed among the subjects.

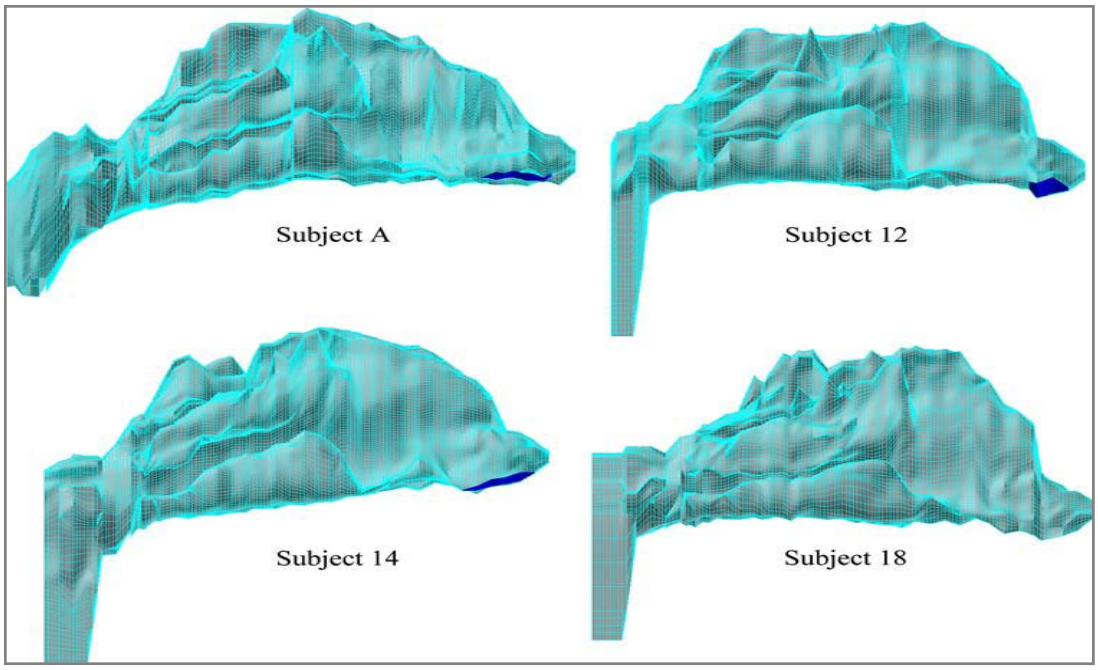

Figure 2.6: Computational meshes for subjects A, 12, 14 and 18. Nostrils are shown in blue on the right side of the models and the nasopharynx is on the left- reproduced from Segal et al., (2008)

Wen *et al*., (2008) also simulated steady laminar nasal airflow for flow rates of 7.5 to 15L/min using computational fluid dynamics software FLUENT. An anatomically correct three dimensional human nasal cavity computed from CT scan images were used (see Figure 2.7). The solution was found to be mesh-independent at approximately 950,000 cells. Results shows that the nasal resistance value within the first 2-3 cm contribute up to 50% of the total airway resistance. Vortices were observed in the upper olfactory region and just after the nasal valve region.

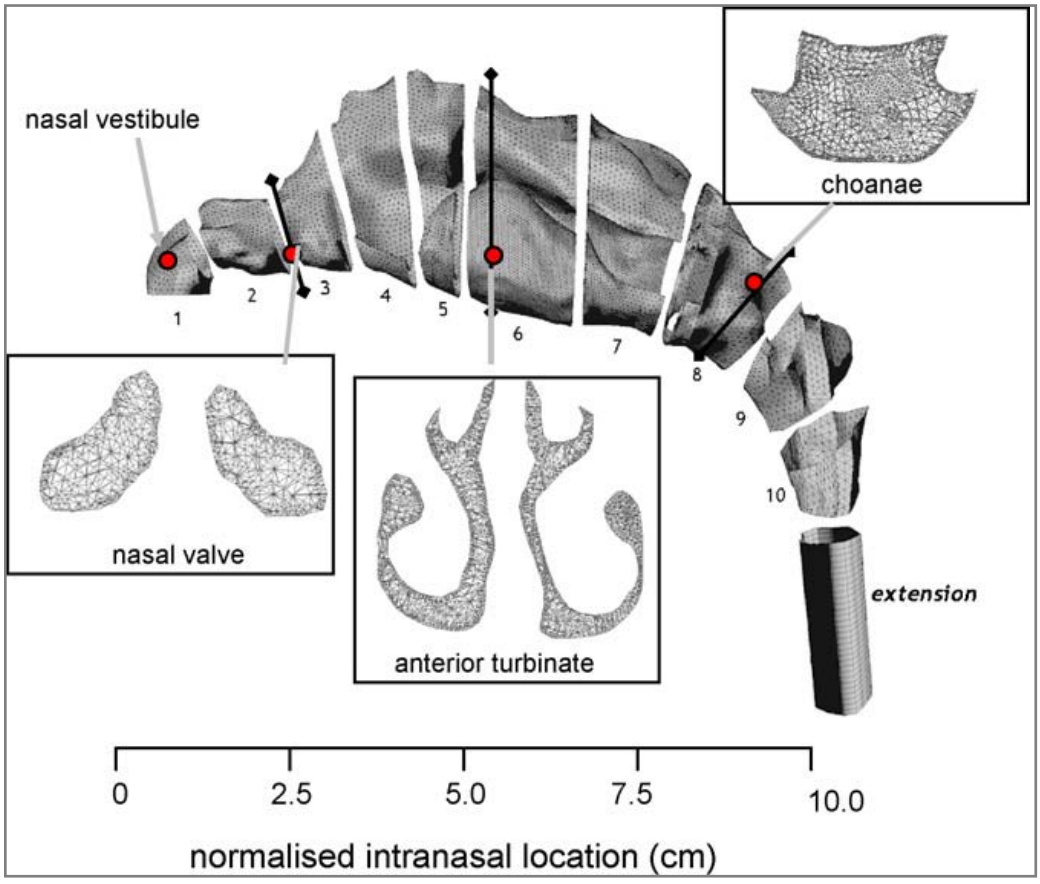

Figure 2.7: Nasal cavity model constructed by Wen et al., (2008)

Inthavong *et al*., (2007) constructed 3D nasal passage based on nasal geometry which obtained through a CT scan of a healthy human nose. A constant laminar flow

rates about 7.5 L/min was used to simulate light breathing. The mesh in the computational domain is unstructured tetrahedral and the size of the mesh is approximately 950,000 cells. The airflow analysis showed vortices present in nasal valve region which enhanced fibre deposition by trapping and recirculating the fibre in the regions where the axial velocity is low.

Another work was done by Croce *et al*., (2006), who also simulated steady state inspiratory laminar airflow for flow rate of 353 ml/s in both nostril using FLUENT. The 3D computational geometry used in Croce *et al*., (2006) numerical study was derived from CT scan images of a plastinated head using a commercial software package, AMIRA (Mercury Computer System, Berlin). The final adapted mesh consisted of 1,353,795 tetrahedral cells. The results obtained from this study shows that airflow was predominant in the inferior median part of nasal cavities. Vortices were observed downstream from the nasal valve and toward the olfactory region.

Other studies include Zamankhan *et al*., (2006), who study the flow and transport and deposition of nano-size particle in a three dimensional model of human nasal passage. The nasal cavity model was contructed from a series of coronal MRI scans. They simulated the steady state flows for breathing rate of 14 L/min and the Reynolds number bases on the hydraulic diameter was about 490. The airflow simulation results were compared with the available experimental data for the nasal passage. They found that, despite the anatomical differences of the human subjects used in the experiments and computer model, the simulation results were in qualitatively agreed with the experimental data.

Several researchers treated the nasal airflow as turbulent flow. Liu *et al*., (2007) constructed 3D human nose model based on coronal CT scans. A nostril pointing downwards was added to the nasal geometry model. Unstructured mesh were created with the size of the mesh was approximately 4,000,000 elements. Turbulent flows were simulated for inhalation flow rates ranging from 7.5 to 60 L/min by using Reynolds Averaged Navier-Stokes (RANS)/ Eddy Interaction Model (EIM). Large Eddy Simulation (LES) modelling was simulated for intermediates flow rates of 30 and 45 L/min. The simulations study showed that the total particle deposition result using LES indicate that the particle deposition efficiency in the nasal cavity show better agreement than standard RANS/EIM approach when compared to the in vivo data.

Zhao *et al*., (2006) also treated the nasal airflow as turbulent in their study. They constructed 3D nasal model based on CT scans in order to investigate the left nasal valve airway which was partially obstructed. Then, they modified the nasal valve region volume to simulate the narrowing of the nasal valve during human sniffing. The airflow was assumed as turbulent and total nasal flow rates was between 300 and 1000ml/s. Result from this study revealed that the increase in airflow rate during sniffing can increase odorant uptake flux to the olfactory mucosa but lower the cumulative total uptake in the olfactory region when the inspired air/odorant volume was held fixed.

Another nasal airflow analysis using the turbulence model was conducted by Mylavarapu *et al*., (2009). They investigated the fluid flow through human nasal airway model which was constructed from axial CT scans. TGRID was then used to create an unstructured hybrid volume mesh with approximately 550,000 cells. Flow simulations and experiments were performed for flow rate of 200 L/min during expiration. Several different numerical approaches within the FLUENT commercial software framework

were used in the simulations; unsteady Large Eddy Simulation (LES), steady Reynolds-Averaged Navier-Stokes (RANS) with two-equation turbulence models (i.e. k-epsilon, standard k-omega, and k-omega Shear Stress Transport (SST)) and with one-equation Spalart-Allmaras model. Among all the approaches, standard k-omega turbulence model resulted in the best agreement with the static pressure measurements, with an average error of approximately 20% over all ports. The largest pressure drop was observed at the tip of the soft palate. This location has the smallest cross section of the airway.

Numerical study on human nasal airflow with abnormal nasal cavity cause by several chronic diseases also has been the subject of several studies. Wexler *et al*., (2005) constructed 3D nasal model of a patient with sinonasal disease. They investigated the aerodynamic consequences of conservative unilateral inferior turbinate reduction using computational fluid dynamics (CFD) methods to accomplish detailed nasal airflow simulations. Steady-state, inspiratory laminar airflow simulations were conducted at 15L/min. They found that inferior turbinate reduce the pressure along the nasal airway. Also, the airflow was minimally affected in the nasal valve region, increased in the lower portion of the middle and posterior nose, and decreased dorsally.

Garcia *et al*., (2007) constructed 3D nasal geometry by using medical imaging software (MIMICs, Materialise) to investigate airflow, water transport, and heat transfer in the nose of an Atrophic Rhinitis (AR). The patient underwent a nasal cavity-narrowing procedure. Rib cartilage was implanted under the mucosa along the floor of the nose, and septum spur was removed. The reconstructed nose was simulated and the nasal airflow was assumed as laminar with 15 L/min corresponding to resting breathing rate. This study showed that the atrophic nose geometry had a much lower surface area

than the healthy nasal passages. The simulations indicated that the atrophic nose did not condition inspired air as effectively as the healthy geometries.

Lindemann *et al*., (2005) produced 3D model of human nose to investigate the intranasal airflow after radical sinus surgery. The human nasal model was constructed based on CT scans of the nasal cavities and the paranasal sinuses of an adult. The numerical simulation was performed by assuming the nasal airflow as laminar at 14 L/min for quiet breathing rate. Result showed that aggressive sinus surgery with resection of the lateral nasal wall complex and the turbinates cause disturbance of the physiological airflow, an enlargement of the nasal cavity volume, as well as an increase in the ratio between nasal cavity volume and surface area.

2.5 Gender comparison

Several researchers have shown the benefits of computational fluid dynamics (CFD) in better understanding of flow through the nasal cavity. Some of the main players are Wen *et al*., (2008), Mylavarapu *et al*., (2009), Segal *et al*., (2008), Weinhold *et al*., (2004), Xiong *et al*., (2008). However, most of the researchers employed male human subject in the determination of the nasal patency. Inter human anatomical differences exists and also differences on anatomical and physiological morphology are observed based on gender. No specific numerical modelling studies have been carried out to compare and ascertain the effect of gender on flow variable inside the nasal cavity. Gender differences is said to be the important determinant of clinical manifestations of airway disease. Even though obstructive sleep apnea, is prevalent in both the gender, its effect on male subjects is more prominently observed (Rowley *et al*.,

2002). Also a higher prevalence of irregular breathing phenomenon among men when compared to women during sleeping and also the fact that men have a larger upper airways in sitting and supine positions (Thurnheer *et al*., 2001) makes it all the more important to study the effect of gender on breathing phenomenon. It would be an importance too to study the effect of anatomical variation based on gender on the flow parameter.

2.6 Gravity Effect

Also CFD modelling involves various simplifications, for example the postural effects which drastically affect the outcome of the analysis. The postural changes in nasal airway resistances are of clinical importance when accessing patients with nasal obstruction. Mohsenin, (2003) demonstrated the effect of decrease in pharyngeal cross sectional area and occurrence of OSA. The gravitational force is considered to be one significant determinant of the closing pressure (Watanabe *et al*., 2002). Study performed by Tvinnereim *et al*., (1996) showed that nasal and pharyngeal resistance doubles upon assumption of supine posture; however the difference obtained was not statistically significant. Beaumont *et al*., (1998) found that at sea level, gravity forces that cause the soft palate and tongue to fall back in the supine posture would narrow upper airways in all its length. A study by Hsing-won Wang, (2002) on the effect of posture on nasal resistance varied from 0.612 Pa/mL/sec in sitting position to 0.663Pa/mL/sec in the supine position.

Matsuzawa *et al*., (1995) observed that the MRI data obtained in supine, lateral and prone position revealed that the upper airway was narrowest in the supine position, and widest in the prone position indicating the anatomical narrowing of the upper airway especially the pharyngeal area. Martin *et al*., (1995) showed in the supine position all the upper airway dimensions decreases with increasing age in both men and women, except the oropharyngeal junction. Hence, it is very important to study the effect of gravity on the flow through the nasal cavity.

2.7 Plug flow and pull flow boundary condition

Keyhani *et al*., (1995), Wexler *et al*., (2005), Zamankhan *et al*., (2006), Segal *et al*., (2008), and Ishikawa *et al*., (2009) constructed 3D nasal computational models and simulated the airflow by utilizing plug flow boundary condition. For plug flow, fixed airflow rate with a uniform velocity profile was imposed at the nostril. While a stress free boundary condition was used at the outflow boundary condition. On the other hand, the pull flow boundary condition is based on negative pressure set at the nasopharynx. Garcia *et al*., (2007) used pull flow boundary condition to study the airflow and water transport simulation in the nasal cavity. Wexler *et al*., (2005) also attempted to conduct the nasal airflow simulation using pull flow boundary condition. However, this simulation has been unsuccessful due to the failure of residuals to converge. There is still no unanimity among the researchers with respect to the use of exact boundary conditions. Most researchers employed the plug flow model in order to stimulate the flow features inside the nasal cavity. The natural physiological inspiratory mechanism is based on pull flow conditions, wherein the expansion of the lungs sets in negative

pressure gradient enabling the air from the ambient atmosphere to rush inside the nasal cavity through the nostril inlets.

2.8 Summary

In summary, the literature reviewed shows that all the previous numerical studies on nasal airflow have generalized the behavior to both gender. No specific numerical modelling studies have been carried out to compare and ascertain the effect of gender on flow variable inside the nasal cavity. Also CFD modelling involves various simplifications, for example the postural effects which drastically affect the outcome of the analysis. It was also found that there is no unanimity with respect to the use of exact boundary conditions. Hence there is no standardization of the boundary definition with respect to the study concerning the nasal flow using numerical methods. Therefore the current work will investigate the effect of different boundary condition on nasal airflow behavior through the human nasal cavity. Also the effects of gravity and posture on flow properties inside the nasal cavity will be investigated. Finally, the gender effect on nasal airflow characteristic due to variation in nasal anatomy will be studied.

CHAPTER 3

METHODOLOGY

3.1 Overview

This chapter presents the method used to reconstruct the three-dimensional model of the human nasal cavity, mesh generation and numerical setup for the nasal airflow simulation. The overall process of the present numerical study has been illustrated in the flow chart below.

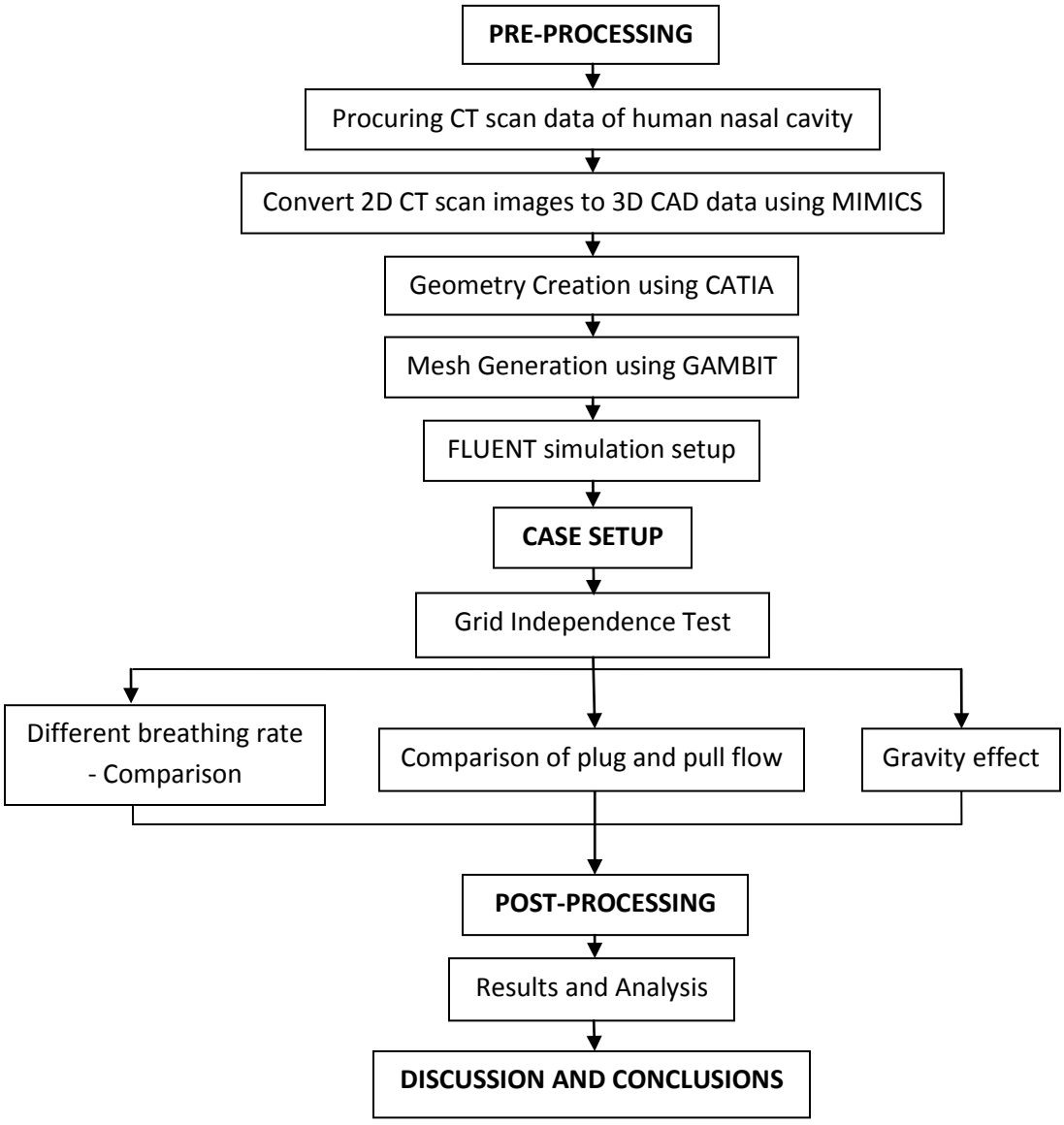

3.2 3D computational model of the nasal cavity

Reconstruction of 3D anatomical model of the human nasal cavity can be very time consuming. The general process of developing the 3D anatomical model basically consist of selection of CT scan data of human nasal cavity followed by converting the 2D CT scan images into 3D CAD data using medical image processing software, MIMICs and finally construct the surface geometry by using CAD software, CATIA.

3.2.1 Procuring CT scan data of human nasal cavity

The anatomical model of the nasal airway used for this numerical study was derived from CT scan images of a healthy 39 year old Malaysian female. The CT scan image of the nasal airway was taken from pre-existing CT scan data sourced from Universiti Sains Malaysia, Medical Campus Hospital. The nasal anatomy was attested to be normal by the ear, nose and throat (ENT) surgeon. Figure 3.1 shows a series of coronal CT scan images along the axial distance of the nasal cavity of the female human subject. The scans produced a total 385 slices of axial, coronal and sagittal images which accounted for the complete nasal cavity area, from nostril to nasopharynx.

The increment between each slice of the scan images is 0.8mm and the scan pixel resolution is 0.434mm. It is important to make sure that the scan interval is less than 2 mm in order to accurately capture the complex geometry of the nasal cavity and to avoid stair-step artifact which usually appear on the curved surface of the model (Bailie *et al*., 2006). However, reduction of the layer thickness requires more expensive machines and a slower build process. The CT scan data was imported into medical image processing

software MIMICs for the reconstruction of the 3D human nasal cavity for this case study.

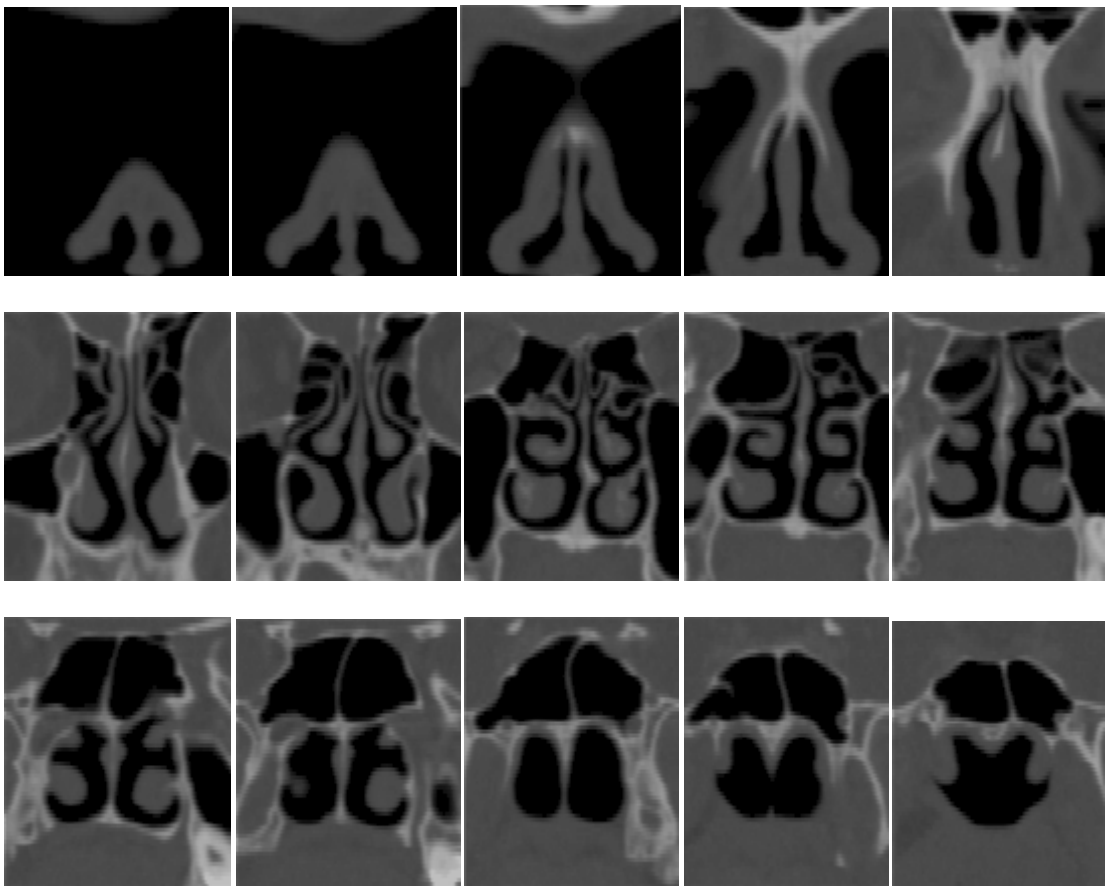

Figure 3.1: Coronal CT scan images along the axial distance of the human nasal cavity

3.2.2 Convert 2D CT scan images to 3D CAD data using MIMICs

MIMICs is an image processing and editing software which provides the tool for the visualization and segmentation of CT images and also for the 3D rendering of objects. Before the scan data can be processed, MIMICs reads the 2D CT scan images from the DICOM (*.dcm) file format and convert it into MIMICs (*.mcs) file format.